

# Searching for Dark Matter in Unification Models: A Hint from Indirect Sensitivities towards Future Signals in Direct Detection and B-decays<sup>1</sup>

Keith A. Olive

*William I Fine Theoretical Physics Institute,  
 University of Minnesota, Minneapolis, MN 55455, USA*

**Abstract.** A comparison is made between accelerator and direct detection constraints in constrained versions of the minimal supersymmetric standard model. Models considered are based on mSUGRA, where scalar and gaugino masses are unified at the GUT scale. In addition, the mSUGRA relation between the (unified)  $A$  and  $B$  parameters is assumed, as is the relation between  $m_0$  and the gravitino mass. Also considered are models where the latter two conditions are dropped (the CMSSM), and a less constrained version where the Higgs soft masses are not unified at the GUT scale (the NUHM).

**Keywords:** Dark Matter; Supersymmetry

**PACS:** 11.30Pb, 13.25.Hw, 95.35.+d, 98.80.-k

## UNIFICATION MODELS

As constraints from accelerator searches and direct detection experiments improve, and in anticipation of the potential for discovery at the LHC, it worthwhile comparing what we can extract from existing data. I will assume several unification conditions placed on the supersymmetric parameters. In all models considered, the gaugino masses are assumed to be unified at the GUT scale with value,  $m_{1/2}$ , as are the trilinear couplings with value  $A_0$ . Also common to all models considered here is the unification of all sfermion masses set equal to  $m_0$  at the GUT scale. In the most constrained scenarios [1], I will apply the full set of conditions which are derived in minimal supergravity models (mSUGRA) [2]. In addition to the conditions listed above, these include, the unification of all scalar masses (including the Higgs soft masses), a relation between the bilinear and trilinear couplings  $B_0 = A_0 - m_0$ , and the relation between the gravitino mass and soft scalar masses,  $m_{3/2} = m_0$ . When electroweak symmetry breaking boundary conditions

---

<sup>1</sup> Summary of talk given at the International Workshop The Dark Side Side of the Universe - DSU2006, Univerisdad Autonoma de Madrid, June 2006.

are applied, this theory contains only  $m_{1/2}, m_0$ , and  $A_0$  in addition to the sign of the Higgs mixing mass,  $\mu$ , as free parameters. The magnitude of  $\mu$  as well as  $\tan\beta$  are predicted.

The extensively studied [3] constrained version of the MSSM or CMSSM drops the latter two conditions. Namely,  $B_0$  and the gravitino mass are not fixed by other parameters. As a result,  $\tan\beta$  becomes a free parameter (as does the gravitino mass). Finally, I will also discuss a less constrained model, the NUHM, in which the Higgs soft masses are not unified at the GUT scale [4, 5]. In this class of models, both  $\mu$  and the Higgs pseudo scalar mass become free parameters.

## INDIRECT SENSITIVITIES

Measurements at low energies can provide interesting indirect information about the supersymmetric parameter space. For example, data obtained at the Brookhaven  $g_\mu - 2$  experiment [6] favored distinct regions of parameter space [7]. Present data on observables such as  $M_W$ ,  $\sin^2 \theta_{\text{eff}}$ , and  $\text{BR}(b \rightarrow s\gamma)$  in addition to  $(g_\mu - 2)$  already provide interesting information on the scale of supersymmetry (SUSY) [8, 9]. The non-discovery of charginos and the Higgs boson at LEP also imposes significant lower bounds on  $m_{1/2}$ .

An important further constraint is provided by the density of dark matter in the Universe, which is tightly constrained by the three-year data from WMAP [10] which has determined many cosmological parameters to unprecedented precision. In the context of the  $\Lambda$ CDM model, the WMAP only results indicate

$$\Omega_m h^2 = 0.1268^{+0.0072}_{-0.0095} \quad \Omega_b h^2 = 0.02233^{+0.00072}_{-0.00091} \quad (1)$$

The difference corresponds to the requisite dark matter density

$$\Omega_{\text{CDM}} h^2 = 0.1045^{+0.0072}_{-0.0095} \quad (2)$$

or a  $2\sigma$  range of  $0.0855 - 0.1189$  for  $\Omega_{\text{CDM}} h^2$ .

The dark matter constraint has the effect within the CMSSM, assuming that the dark matter consists largely of neutralinos [11], of restricting  $m_0$  to very narrow allowed strips for any specific choice of  $A_0$ ,  $\tan\beta$  and the sign of  $\mu$  [12, 13]. These strips are typically due to co-annihilation processes between the neutralino and stau [14]. Shown in Fig. 1 are the WMAP lines [12] of the  $(m_{1/2}, m_0)$  plane allowed by the cosmological constraint and laboratory constraints for  $\mu > 0$  and values of  $\tan\beta$  from 5 to 55, in steps  $\Delta(\tan\beta) = 5$ . We notice immediately that the strips are considerably narrower than the spacing between them, though any intermediate point in the  $(m_{1/2}, m_0)$  plane would be compatible with some intermediate value of  $\tan\beta$ . The right (left) ends of the strips correspond to the maximal (minimal) allowed values of  $m_{1/2}$  and hence  $m_\chi$ . The lower bounds on  $m_{1/2}$  are due to the Higgs mass constraint for  $\tan\beta \leq 23$ , but are determined by the  $b \rightarrow s\gamma$  constraint for higher values of  $\tan\beta$ . Thus, the dimensionality of the supersymmetric parameter space is further reduced, and one may explore supersymmetric phenomenology along these ‘WMAP strips’, as has already been done for the direct detection of supersymmetric particles at the LHC and linear colliders of varying energies [15, 16].

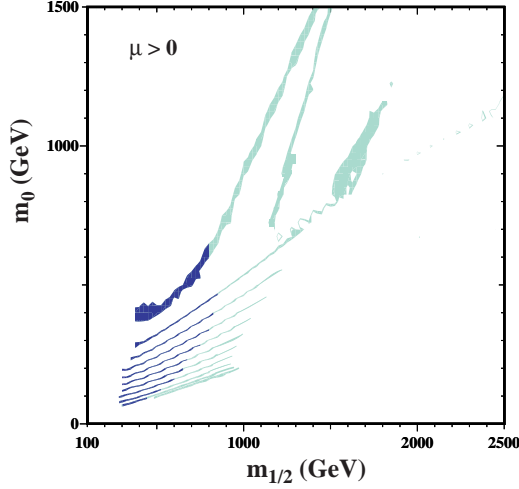


**FIGURE 1.** The strips display the regions of the  $(m_{1/2}, m_0)$  plane that are compatible with  $0.094 < \Omega_\chi h^2 < 0.129$  and the laboratory constraints for  $\mu > 0$  and  $\tan\beta = 5, 10, 15, 20, 25, 30, 35, 40, 45, 50, 55$ . The parts of the strips compatible with  $g_\mu - 2$  at the 2- $\sigma$  level have darker shading.

Another mechanism for extending the allowed CMSSM region to large  $m_\chi$  is rapid annihilation via a direct-channel pole when  $m_\chi \sim \frac{1}{2}m_A$  [17, 18]. Since the heavy scalar and pseudoscalar Higgs masses decrease as  $\tan\beta$  increases, eventually  $2m_\chi \simeq m_A$  yielding a ‘funnel’ extending to large  $m_{1/2}$  and  $m_0$  at large  $\tan\beta$ , as seen in the high  $\tan\beta$  strips of Fig. 1.

For large values of  $\tan\beta$ , particularly when  $m_A$  is small, supersymmetry leads to an enhancement in an otherwise rare decay of the  $B$  meson, namely  $B_s \rightarrow \mu^+ \mu^-$ . The decay  $B_s \rightarrow \mu^+ \mu^-$  is known to impose another interesting constraint on the parameter spaces of models for physics beyond the Standard Model, such as the MSSM [19, 20, 21]. The Fermilab Tevatron collider already has an interesting upper limit  $\sim 2 \times 10^{-7}$  on the  $B_s \rightarrow \mu^+ \mu^-$  decay branching ratio [22], and future runs of the Fermilab Tevatron collider and the LHC are expected to increase significantly the experimental sensitivity to  $B_s \rightarrow \mu^+ \mu^-$  decay. Indeed, the latest CDF limit [23], is now  $1 \times 10^{-7}$  at the 95% CL. Currently,  $B_s \rightarrow \mu^+ \mu^-$  does not provide strong constraints in the CMSSM [20]. However, as we will see, in the NUHM, current experimental limits already exclude interesting models [21].

Finally, there is one additional region of acceptable relic density known as the focus-point region [24], which is found at very high values of  $m_0$ . As  $m_0$  is increased, the solution for  $\mu$  at low energies as determined by the electroweak symmetry breaking conditions eventually begins to drop. When  $\mu \lesssim m_{1/2}$ , the composition of the LSP gains a strong Higgsino component and as such the relic density begins to drop precipitously. As  $m_0$  is increased further, there are no longer any solutions for  $\mu$ .

In [8, 9] we considered the following observables: the  $W$  boson mass,  $M_W$ , the effective weak mixing angle at the  $Z$  boson resonance,  $\sin^2 \theta_{\text{eff}}$ , the anomalous magnetic moment of the muon,  $(g_\mu - 2)$  (we used the SM prediction based on the  $e^+e^-$  data for the hadronic vacuum polarization contribution [25]) and the rare  $b$  decays  $\text{BR}(b \rightarrow s\gamma)$ ,

as well as the mass of the lightest  $CP$ -even Higgs boson,  $m_h$ .

We performed the analysis of the sensitivity to  $m_{1/2}$  moving along the WMAP strips with fixed values of  $A_0$  and  $\tan\beta$ . The experimental central values, the present experimental errors and theoretical uncertainties are as described in [8, 9]. Assuming that the five observables are uncorrelated, a  $\chi^2$  fit has been performed with

$$\chi^2 \equiv \sum_{n=1}^4 \left( \frac{R_n^{\text{exp}} - R_n^{\text{theo}}}{\sigma_n} \right)^2 + \chi_{m_h}^2 \quad (3)$$

Here  $R_n^{\text{exp}}$  denotes the experimental central value of the  $n$ th observable,  $R_n^{\text{theo}}$  is the corresponding theoretical prediction,  $\sigma_n$  denotes the combined error, and  $\chi_{m_h}^2$  denotes the  $\chi^2$  contribution coming from the lightest MSSM Higgs boson mass [9].

Our final analysis ingredient is the elastic scattering cross section between a neutralino and the proton, which is tested by direct detection experiments. The following low-energy effective four-fermion Lagrangian describes spin-independent elastic  $\chi$ -nucleon scattering:

$$\mathcal{L} = \alpha_{3i} \bar{\chi} \chi \bar{q}_i q_i, \quad (4)$$

which is to be summed over the quark flavours  $q$ , and the subscript  $i$  labels up-type quarks ( $i = 1$ ) and down-type quarks ( $i = 2$ ). Expressions for  $\alpha_{3i}$  can be found in [26]. The scalar part of the cross section can be written as

$$\sigma_3 = \frac{4m_r^2}{\pi} [Zf_p + (A - Z)f_n]^2, \quad (5)$$

where  $m_r$  is the reduced LSP mass,

$$\frac{f_p}{m_p} = \sum_{q=u,d,s} f_{Tq}^{(p)} \frac{\alpha_{3q}}{m_q} + \frac{2}{27} f_{TG}^{(p)} \sum_{c,b,t} \frac{\alpha_{3q}}{m_q}, \quad (6)$$

the parameters  $f_{Tq}^{(p)}$  are defined by

$$m_p f_{Tq}^{(p)} \equiv \langle p | m_q \bar{q} q | p \rangle \equiv m_q B_q, \quad (7)$$

$f_{TG}^{(p)} = 1 - \sum_{q=u,d,s} f_{Tq}^{(p)}$  [27], and  $f_n$  has a similar expression. This may be determined from the  $\pi$ -nucleon  $\Sigma$  term, which is given by

$$\sigma_{\pi N} \equiv \Sigma = \frac{1}{2} (m_u + m_d) (B_u + B_d). \quad (8)$$

and carries substantial uncertainties [26]. Here we will consider  $\Sigma = 45$  and  $64$  GeV.

## MSUGRA MODELS

We begin the discussion of unifications models, with the most constrained version of the MSSM, based on mSUGRA, labelled here as the VCMSSM [1]. Recall that in these

models,  $\tan\beta$  is fixed by the electroweak boundary conditions, and values of  $\tan\beta$  are generally below 35 for most of the  $m_{1/2}, m_0$  planes which are now characterized by  $A_0/m_0$ . As a result, relic density funnels do not appear, nor is the focus point ever reached. The signal from  $B_s \rightarrow \mu^+ \mu^-$  is very weak and direct detection experiments are only beginning to sample these models (see below for the CMSSM).

Fig. 2 displays the  $\chi^2$  function for a sampling of gravitino dark matter (GDM) scenarios [28] obtained by applying the supplementary gravitino mass condition to VCMSSM models for  $A_0/m_0 = 0, 0.75, 3 - \sqrt{3}$  and 2, and scanning the portions of the  $m_{1/2}, m_0$  planes with GDM at low  $m_0$  [9]. These wedges are scanned via a series of points at fixed (small)  $m_0$  and increasing  $m_{1/2}$ . As seen in Fig. 2, the global minimum of  $\chi^2$  for all the VCMSSM models with gravitino dark matter (GDM) with  $A_0/m_0 = 0, 0.75, 3 - \sqrt{3}$  and 2 is at  $m_{1/2} \sim 450$  GeV. As a consequence, there are good prospects for observing the gluino and perhaps the stop at the LHC. We recall that, in these GDM scenarios, the  $\tilde{\tau}_1$  is the NLSP, and that the  $\tilde{\chi}_1^0$  is heavier. The  $\tilde{\tau}_1$  decays into the gravitino and a  $\tau$ , and is metastable with a lifetime that may be measured in hours, days or weeks. Specialized detection strategies for the LHC were discussed in [29]: this scenario would offer exciting possibilities near the  $\tilde{\tau}_1$  pair-production threshold at the ILC.

The results indicate that, already at the present level of experimental accuracies, the electroweak precision observables combined with the WMAP constraint provide a sensitive probe of the VCMSSM, yielding interesting information about its parameter space. The rise in  $\chi^2$  at low  $m_{1/2}$  is primarily due to the constraint from  $m_h$ , whereas at high  $m_{1/2}$ , the rise is due to the discrepancy between the  $g_\mu - 2$  measurement and the standard model calculation. Also important however are the contributions from  $M_W$  and  $\sin^2 \theta_{\text{eff}}$  as will be seen in the analogous discussion for the VCMSSM.

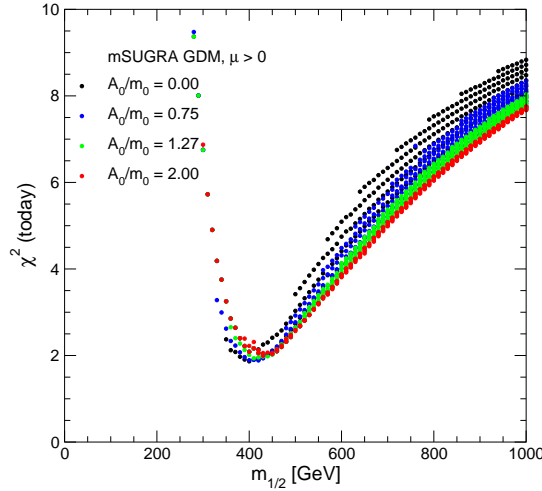


**FIGURE 2.** The dependence of the  $\chi^2$  function on  $m_{1/2}$  for GDM scenarios with  $A_0/m_0 = 0, 0.75, 3 - \sqrt{3}$  and 2, scanning the regions where the lighter stau  $\tilde{\tau}_1$  is the NLSP.

As discussed above, a feature of the class of GDM scenarios discussed here is that the required value of  $\tan\beta$  increases with  $m_{1/2}$ . Therefore, the preference for relatively small  $m_{1/2}$  discussed above maps into an analogous preference for moderate  $\tan\beta$ . We

found that, at the 95% confidence level

$$300\text{GeV} \lesssim m_{1/2} \lesssim 800\text{GeV}, \quad 15 \lesssim \tan\beta \lesssim 27 \quad (9)$$

in this mSUGRA class of GDM models.

## THE CMSSM

When we drop the conditions on  $B_0$  and  $m_{3/2}$ , we recover the well studied CMSSM.  $\tan\beta$  is now a free parameter, and we will assume that the gravitino is suitably heavy so as to allow for neutralino dark matter. For a given value of  $\tan\beta$  and  $A_0$ , the relic density can be used to fix  $m_0$  as a function of  $m_{1/2}$  producing the WMAP strips seen in Fig. 1. The first panel of Fig. 3, displays the behaviour of the  $\chi^2$  function out to the tips of typical WMAP coannihilation strips. As one can see, there is a pronounced minimum in  $\chi^2$  as a function of  $m_{1/2}$  for  $\tan\beta = 10$ . The  $\chi^2$  curve depends strongly on the value of  $A_0$ , corresponding to its strong impact on  $m_h$ . Values of  $A_0/m_{1/2} < -1$  are disfavoured at the 90% C.L., essentially because of their lower  $m_h$  values, but  $A_0/m_{1/2} = 2$  and 1 give equally good fits and descriptions of the data. The constraint due to  $m_h$  is chiefly responsible for the sharp rise in  $\chi^2$  at low  $m_{1/2}$ .

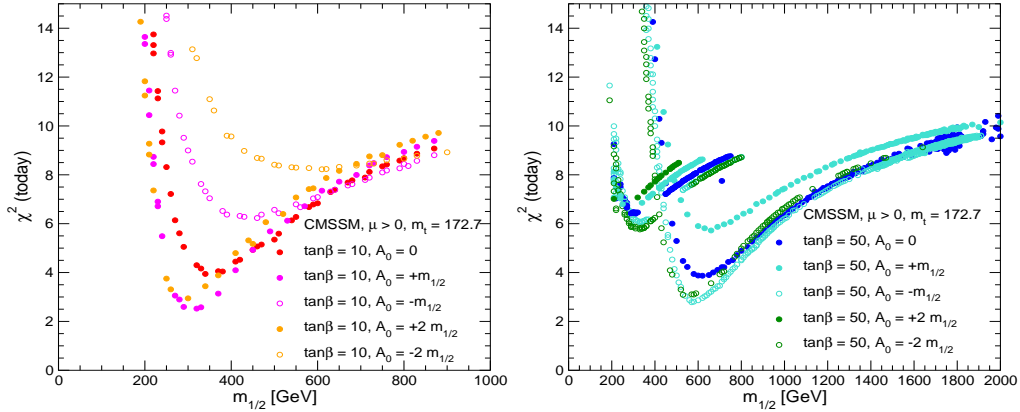


**FIGURE 3.** The combined likelihood function  $\chi^2$  for the electroweak observables  $M_W$ ,  $\sin^2 \theta_{\text{eff}}$ ,  $(g-2)_\mu$ ,  $\text{BR}(b \rightarrow s\gamma)$ , and  $m_h$  evaluated in the CMSSM for  $\tan\beta = 10$  (a) and 50 (b),  $m_t = 172.7 \pm 2.9$  GeV and various discrete values of  $A_0$ , with  $m_0$  then chosen to yield the central value of the relic neutralino density indicated by WMAP and other observations.

At large  $m_{1/2}$ , the increase in  $\chi^2$  is largely due to  $g_\mu - 2$ , but also has sizable contributions from the observables  $M_W$  and  $\sin^2 \theta_{\text{eff}}$ . The importance of these latter two observables has grown with recent determinations of  $m_t$ . The previous range  $m_t = 178.0 \pm 4.3$  GeV [30] has evolved to  $172.7 \pm 2.9$  GeV [31] (and very recently to  $172.5 \pm 2.3$  GeV [32] and even more recently to  $171.4 \pm 2.3$  GeV [33]). The effect of this lower  $m_t$  value is twofold [34].

First, it drives the SM prediction of  $M_W$  and  $\sin^2 \theta_{\text{eff}}$  further away from the current experimental value <sup>2</sup>. This effect is shown in Fig. 4 for  $\tan \beta = 10$ . The change in the SM prediction elevates the experimental discrepancy to about  $1.5 \sigma$ , despite the change in the preferred experimental range of  $M_W$ , which does not compensate completely for the change in  $m_t$ . The net effect is therefore to increase the favoured magnitude of the supersymmetric contribution, i.e., to lower the preferred supersymmetric mass scale. In the case of  $\sin^2 \theta_{\text{eff}}$ , the reduction in  $m_t$  has increased the SM prediction whereas the experimental value has not changed significantly. Once again, the discrepancy with the SM has increased to about  $1.5 \sigma$ , and the preference for a small value of  $m_{1/2}$  has therefore also increased. With the new lower experimental value of  $m_t$ ,  $M_W$  and  $\sin^2 \theta_{\text{eff}}$  give substantial contributions, adding up to more than 50% of the  $(g-2)_\mu$  contribution to  $\chi^2$  at the tip of the WMAP strip. Secondly, the predicted value of the lightest Higgs boson mass in the MSSM is lowered by the new  $m_t$  value. As a result, the LEP Higgs bounds [35] now impose a more important constraint on the MSSM parameter space, notably on  $m_{1/2}$ .

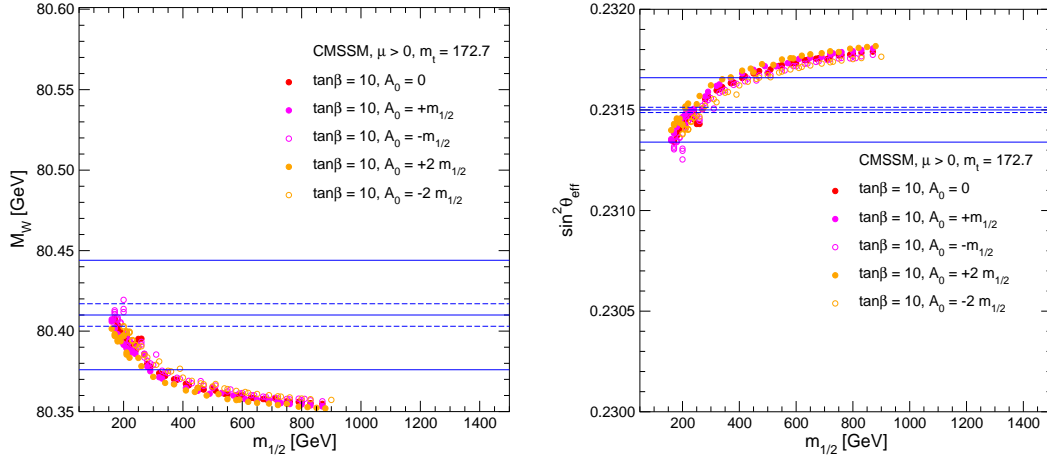


**FIGURE 4.** The CMSSM predictions for  $M_W$  (a) and  $\sin^2 \theta_{\text{eff}}$  (b) as functions of  $m_{1/2}$  for  $\tan \beta = 10$  for various  $A_0$ . The top quark mass has been set to  $m_t = 172.7$  GeV. The current experimental measurements indicated in the plots are shown by the solid lines. Future ILC sensitivities are estimated by the dashed lines.

The corresponding results for WMAP strips in the coannihilation, Higgs funnel and focus-point regions for the case  $\tan \beta = 50$  are shown in Fig. 3b. The spread of points with identical values of  $A_0$  at large  $m_{1/2}$  is due to the broadening and bifurcation of the WMAP strip in the Higgs funnel region. With the lower value of  $m_t$ , there is the appearance of a group of points with moderately high  $\chi^2$  that have relatively small  $m_{1/2} \sim 200$  GeV. These points have relatively large values of  $m_0$  and are located in the focus-point region of the  $(m_{1/2}, m_0)$  plane [24]. By comparison with our previous analysis, the focus-point region appears at considerably lower values of  $m_0$ , because of the reduction in the central value of  $m_t$ . This focus-point strip extends to larger values of  $m_0$  and hence  $m_{1/2}$  that are not shown. The least-disfavoured focus points have a  $\Delta\chi^2$  of

<sup>2</sup> Whereas  $(g-2)_\mu$  and  $\text{BR}(b \rightarrow s\gamma)$  are little affected.

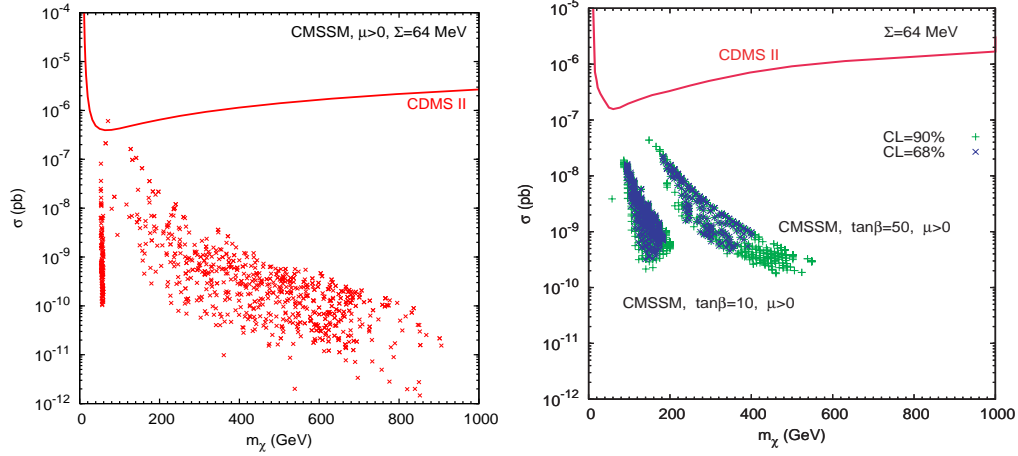


**FIGURE 5.** Scatter plots of the spin-independent elastic-scattering cross section predicted in the CMSSM for  $\tan\beta = 10, \mu > 0$ , with  $\Sigma = 64$  MeV. In panel b, the predictions for models allowed at the 68% (90%) confidence levels are shown by blue  $\times$  signs (green  $+$  signs).

at least 3.3, and most of them are excluded at the 90% C.L.

Taken at face value, the preferred ranges for the sparticle masses shown in Fig. 3 are quite encouraging for both the LHC and the ILC. The gluino and squarks lie comfortably within the early LHC discovery range, and several electroweakly-interacting sparticles would be accessible to ILC(500) (the ILC running at  $\sqrt{s} = 500$  GeV). The best-fit CMSSM point is quite similar to the benchmark point SPS1a [36] (which is close to point benchmark point B [15]) which has been shown to offer good experimental prospects for both the LHC and ILC [37]. The prospects for sparticle detection are also quite good in the least-disfavoured part of the focus-point region for  $\tan\beta = 50$  shown in Fig. 3b, with the exception of the relatively heavy squarks.

Direct detection techniques rely on an ample neutralino-nucleon scattering cross-section. In Fig. 5a, we display the expected ranges of the spin-independent cross sections in the CMSSM when we sample randomly  $\tan\beta$  as well as the other CMSSM parameters [26]. Also shown on the plot is the current CDMS [38] exclusion curve which places an upper limit on the scattering cross section. As one can see, the current limits have only just now begun to probe CMSSM models. CMSSM parameter choices with low  $\chi^2$  based on the indirect sensitivities discussed above are shown in panel b where both the 68% and 95% CL points for  $\tan\beta = 10$  and 50 are displayed. These points remain below current the CDMS sensitivity.

## NUHM MODELS

In the NUHM, we can either choose the two Higgs soft masses as additional free parameters or more conveniently we can choose  $\mu$  and  $m_A$ . The addition of new parameters opens up many possible parameter planes to study. In [9], in addition to  $m_{1/2}, m_0$  planes with non-CMSSM values of  $\mu$  and  $m_A$ ,  $\chi^2$ 's were computed for  $m_{1/2}, \mu$  and  $\mu, m_A$  planes. It was concluded that although the preferred value of the overall sparticle mass



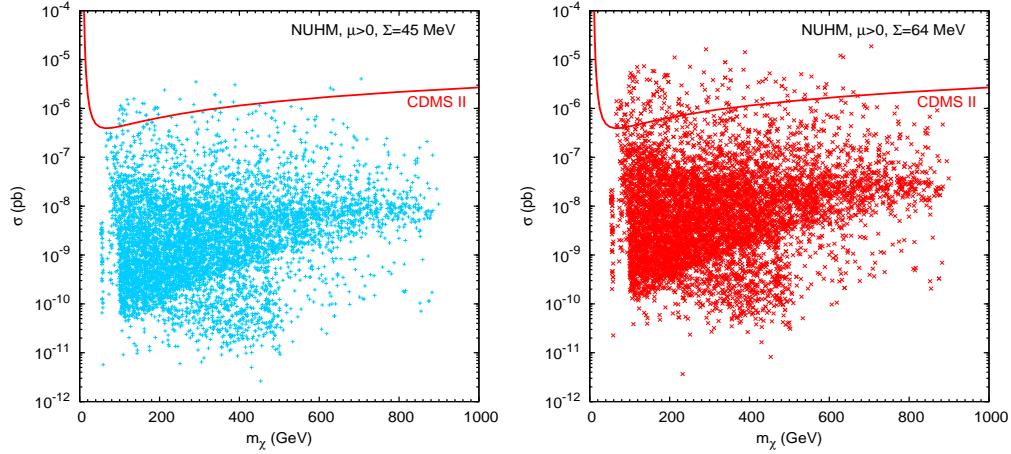


**FIGURE 6.** Scatter plots of the spin-independent elastic-scattering cross section predicted in the CMSSM for (a, b)  $\tan\beta = 10, \mu > 0$  and (c, d)  $\tan\beta = 50, \mu > 0$ , with (a, c)  $\Sigma = 45$  MeV and (b, d)  $\Sigma = 64$  MeV. The predictions for models allowed at the 68% (90%) confidence levels are shown by blue  $\times$  signs (green  $+$  signs).

scale set by  $m_{1/2}$  may be quite similar in the NUHM to its CMSSM value, the masses of some particles in the NUHM may differ significantly from the corresponding CMSSM values.

The NUHM also allows for the possibility of significantly higher elastic cross sections for  $\chi - p$  scattering and current constraints already exclude many interesting models [26]. Furthermore, in those NUHM models which have cross sections in excess of the CDMS limit, one finds relatively low values of  $\mu$  and  $m_A$ .

In Fig. 6, the current CDMS limit is shown compared with a scan over the NUHM parameter space. In panel a, the value of the  $\pi$ -nucleon  $\Sigma$  parameter was taken as 45 MeV and can be compared to panel b, where  $\Sigma = 64$  MeV. The latter clearly shows higher elastic cross sections and represents an inherent uncertainty in the theoretical predictions for these cross sections.

Some specific NUHM ( $\mu, m_A$ ) planes for different values of  $\tan\beta$ ,  $m_{1/2}$  and  $m_0$  are shown in Fig. 7, exhibiting the interplay of the different experimental, phenomenological and theoretical constraints [21]. Each panel features a pair of WMAP strips, above and below the  $m_A = 2m_\chi$  solid (blue) line. The WMAP strip is also seen to follow the brick-red shaded region where the  $\tilde{\tau}_1$  is the LSP. The lower parts of the WMAP strips are excluded by  $B_s \rightarrow \mu^+ \mu^-$  as  $\tan\beta$  increases as seen by the thick black curve which represents the tevatron limit. Here one sees clearly the consequence of the improvement to the CDF bound from  $2$  to  $1 \times 10^{-7}$  as more of the WMAP strip is now excluded. However, in each case sensitivity to  $B_s \rightarrow \mu^+ \mu^-$  below  $10^{-8}$  would be required to explore all of the upper WMAP strip.

Also shown in Fig. 7, is a dashed grey line which is the constraint imposed by the CDMS upper limit on spin-independent elastic cold dark matter scattering. It is interesting to note that the CDMS bound excludes a somewhat larger part of the lower WMAP strip than does  $B_s \rightarrow \mu^+ \mu^-$  for  $\tan\beta = 40$ , whereas the  $B_s \rightarrow \mu^+ \mu^-$  constraint is stronger for  $\tan\beta = 50$ . Most interesting is the result that these two observables are in

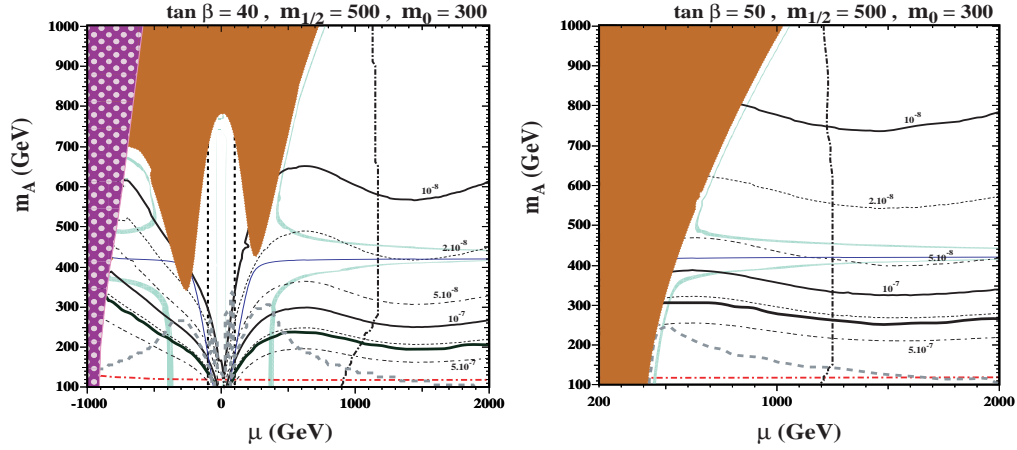


**FIGURE 7.** Allowed regions in the  $(\mu, M_A)$  planes for  $m_{1/2} = 500$  GeV and  $m_0 = 300$  GeV, for (a)  $\tan \beta = 40$ , and (b)  $\tan \beta = 50$ . In each panel, the near-horizontal solid blue line is the contour where  $M_A = 2m_\chi$ , and the turquoise strips are those where the relic neutralino LSP density falls within the range favoured by WMAP and other cosmological and astrophysical observations. The LEP chargino limit is shown as a dashed black line and the GUT stability constraint as a dot-dashed black line. The regions disallowed because the  $\tilde{\tau}_1$  would be the LSP are shaded brick-red. Contours of the  $B_s \rightarrow \mu^+ \mu^-$  branching ratio are labelled correspondingly, with the current Tevatron limit the boldest black line, and the CDMS constraint is shown as a dashed grey line. There is no electroweak symmetry breaking in the polka-dotted region.

fact quite comparable and one can infer from these figures, that the positive detection of either  $B_s \rightarrow \mu^+ \mu^-$  or the direct detection of dark matter should be matched quickly by the detection of the other.

## ACKNOWLEDGMENTS

I would like to thank J. Ellis, S. Heinemeyer, Y. Santoso, V. Spanos, and G. Weiglein for many fruitful collaborations leading to the results summarized here. This work was partially supported by DOE grant DE-FG02-94ER-40823.

## REFERENCES

1. J. R. Ellis, K. A. Olive, Y. Santoso and V. C. Spanos, Phys. Lett. B **573** (2003) 162 [arXiv:hep-ph/0305212]; J. R. Ellis, K. A. Olive, Y. Santoso and V. C. Spanos, Phys. Rev. D **70** (2004) 055005 [arXiv:hep-ph/0405110].
2. R. Barbieri, S. Ferrara and C.A. Savoy, Phys. Lett. **119B** (1982) 343; For reviews, see: H. P. Nilles, Phys. Rep. **110** (1984) 1; A. Brignole, L. E. Ibanez and C. Munoz, arXiv:hep-ph/9707209, published in *Perspectives on supersymmetry*, ed. G. L. Kane, pp. 125-148.
3. J. R. Ellis, G. Ganis and K. A. Olive, Phys. Lett. B **474** (2000) 314 [arXiv:hep-ph/9912324]; V. D. Barger and C. Kao, Phys. Lett. B **518** (2001) 117 [arXiv:hep-ph/0106189]; L. Roszkowski, R. Ruiz de Austri and T. Nihei, JHEP **0108** (2001) 024 [arXiv:hep-ph/0106334]; A. B. Lahanas and V. C. Spanos, Eur. Phys. J. C **23** (2002) 185 [arXiv:hep-ph/0106345]; A. Djouadi, M. Drees and J. L. Kneur, JHEP **0108** (2001) 055 [arXiv:hep-ph/0107316]; U. Chattopadhyay, A. Corsetti and P. Nath, Phys. Rev. D **66** (2002) 035003 [arXiv:hep-ph/0201001]; J. R. Ellis, K. A. Olive and

- Y. Santoso, *New Jour. Phys.* **4** (2002) 32 [arXiv:hep-ph/0202110]; H. Baer, C. Balazs, A. Belyaev, J. K. Mizukoshi, X. Tata and Y. Wang, *JHEP* **0207** (2002) 050 [arXiv:hep-ph/0205325]; R. Arnowitt and B. Dutta, arXiv:hep-ph/0211417.
4. M. Olechowski and S. Pokorski, *Phys. Lett. B* **344**, 201 (1995) [arXiv:hep-ph/9407404]; V. Berezhinsky, A. Bottino, J. Ellis, N. Fornengo, G. Mignola and S. Scopel, *Astropart. Phys.* **5** (1996) 1, hep-ph/9508249; M. Drees, M. Nojiri, D. Roy and Y. Yamada, *Phys. Rev. D* **56** (1997) 276, [Erratum-ibid. **D 64** (1997) 039901], hep-ph/9701219; M. Drees, Y. Kim, M. Nojiri, D. Toya, K. Hasuko and T. Kobayashi, *Phys. Rev. D* **63** (2001) 035008, hep-ph/0007202; P. Nath and R. Arnowitt, *Phys. Rev. D* **56** (1997) 2820, hep-ph/9701301; J. R. Ellis, T. Falk, G. Ganis, K. A. Olive and M. Schmitt, *Phys. Rev. D* **58** (1998) 095002 [arXiv:hep-ph/9801445]; J. R. Ellis, T. Falk, G. Ganis and K. A. Olive, *Phys. Rev. D* **62** (2000) 075010 [arXiv:hep-ph/0004169]; A. Bottino, F. Donato, N. Fornengo and S. Scopel, *Phys. Rev. D* **63** (2001) 125003, hep-ph/0010203; S. Profumo, *Phys. Rev. D* **68** (2003) 015006, hep-ph/0304071; D. Cerdeno and C. Munoz, *JHEP* **0410** (2004) 015, hep-ph/0405057; H. Baer, A. Mustafayev, S. Profumo, A. Belyaev and X. Tata, *JHEP* **0507** (2005) 065, hep-ph/0504001.
  5. J. Ellis, K. Olive and Y. Santoso, *Phys. Lett. B* **539**, 107 (2002) [arXiv:hep-ph/0204192]; J. R. Ellis, T. Falk, K. A. Olive and Y. Santoso, *Nucl. Phys. B* **652**, 259 (2003) [arXiv:hep-ph/0210205].
  6. [The Muon g-2 Collaboration], *Phys. Rev. Lett.* **92** (2004) 161802, hep-ex/0401008; G. W. Bennett *et al.* [Muon G-2 Collaboration], “Final report of the muon E821 anomalous magnetic moment measurement at Phys. Rev. D **73**, 072003 (2006) [arXiv:hep-ex/0602035].
  7. L. L. Everett, G. L. Kane, S. Rigolin and L. Wang, *Phys. Rev. Lett.* **86** (2001) 3484 [arXiv:hep-ph/0102145]; J. L. Feng and K. T. Matchev, *Phys. Rev. Lett.* **86** (2001) 3480 [arXiv:hep-ph/0102146]; E. A. Baltz and P. Gondolo, *Phys. Rev. Lett.* **86** (2001) 5004 [arXiv:hep-ph/0102147]; U. Chattopadhyay and P. Nath, *Phys. Rev. Lett.* **86** (2001) 5854 [arXiv:hep-ph/0102157]; S. Komine, T. Moroi and M. Yamaguchi, *Phys. Lett. B* **506** (2001) 93 [arXiv:hep-ph/0102204]; J. Ellis, D. V. Nanopoulos and K. A. Olive, *Phys. Lett. B* **508** (2001) 65 [arXiv:hep-ph/0102331]; R. Arnowitt, B. Dutta, B. Hu and Y. Santoso, *Phys. Lett. B* **505** (2001) 177 [arXiv:hep-ph/0102344]; S. P. Martin and J. D. Wells, *Phys. Rev. D* **64** (2001) 035003 [arXiv:hep-ph/0103067]; H. Baer, C. Balazs, J. Ferrandis and X. Tata, *Phys. Rev. D* **64** (2001) 035004 [arXiv:hep-ph/0103280].
  8. J. Ellis, S. Heinemeyer, K. Olive and G. Weiglein, *JHEP* **0502** 013 (2005) [arXiv:hep-ph/0411216].
  9. J. R. Ellis, S. Heinemeyer, K. A. Olive and G. Weiglein, *JHEP* **0605**, 005 (2006) [arXiv:hep-ph/0602220].
  10. D. N. Spergel *et al.*, [arXiv:astro-ph/0603449].
  11. J. Ellis, J.S. Hagelin, D.V. Nanopoulos, K.A. Olive and M. Srednicki, *Nucl. Phys. B* **238** (1984) 453; see also H. Goldberg, *Phys. Rev. Lett.* **50** (1983) 1419.
  12. J. R. Ellis, K. A. Olive, Y. Santoso and V. C. Spanos, *Phys. Lett. B* **565** (2003) 176 [arXiv:hep-ph/0303043].
  13. H. Baer and C. Balazs, *JCAP* **0305** (2003) 006 [arXiv:hep-ph/0303114]; A. B. Lahanas and D. V. Nanopoulos, *Phys. Lett. B* **568** (2003) 55 [arXiv:hep-ph/0303130]; U. Chattopadhyay, A. Corsetti and P. Nath, *Phys. Rev. D* **68** (2003) 035005 [arXiv:hep-ph/0303201]; C. Munoz, *Int. J. Mod. Phys. A* **19**, 3093 (2004) [arXiv:hep-ph/0309346]; R. Arnowitt, B. Dutta and B. Hu, arXiv:hep-ph/0310103.
  14. J. R. Ellis, T. Falk and K. A. Olive, *Phys. Lett. B* **444** (1998) 367 [arXiv:hep-ph/9810360]; J. R. Ellis, T. Falk, K. A. Olive and M. Srednicki, *Astropart. Phys.* **13** (2000) 181 [Erratum-ibid. **15** (2001) 413] [arXiv:hep-ph/9905481]; R. Arnowitt, B. Dutta and Y. Santoso, *Nucl. Phys. B* **606** (2001) 59 [arXiv:hep-ph/0102181]; M. E. Gómez, G. Lazarides and C. Pallis, *Phys. Rev. D* **D61** (2000) 123512 [arXiv:hep-ph/9907261]; *Phys. Lett. B* **487** (2000) 313 [arXiv:hep-ph/0004028]; *Nucl. Phys. B* **B638** (2002) 165 [arXiv:hep-ph/0203131]; T. Nihei, L. Roszkowski and R. Ruiz de Austri, *JHEP* **0207** (2002) 024 [arXiv:hep-ph/0206266].
  15. M. Battaglia, A. De Roeck, J. Ellis, F. Gianotti, K. Olive and L. Pape, *Eur. Phys. J. C* **33** (2004) 273, hep-ph/0306219;
  16. H. Baer, A. Belyaev, T. Krupovnickas and X. Tata, *JHEP* **0402** (2004) 007, hep-ph/0311351; J. R. Ellis, K. A. Olive, Y. Santoso and V. C. Spanos, *Phys. Lett. B* **603**, 51 (2004) [arXiv:hep-ph/0408118]. B. Allanach, G. Belanger, F. Boudjema and A. Pukhov, hep-ph/0410091.
  17. H. Baer and M. Brhlik, *Phys. Rev. D* **53** (1996) 597 [arXiv:hep-ph/9508321]; H. Baer, M. Brhlik, M. A. Diaz, J. Ferrandis, P. Mercadante, P. Quintana and X. Tata, *Phys. Rev. D* **63** (2001) 015007 [arXiv:hep-ph/0005027]; A. B. Lahanas and V. C. Spanos, *Eur. Phys. J. C* **23** (2002) 185

- [arXiv:hep-ph/0106345].
18. J. R. Ellis, T. Falk, G. Ganis, K. A. Olive and M. Srednicki, *Phys. Lett. B* **510** (2001) 236 [arXiv:hep-ph/0102098].
  19. A. Dedes, H. K. Dreiner and U. Nierste, *Phys. Rev. Lett.* **87** (2001) 251804 [arXiv:hep-ph/0108037]; R. Arnowitt, B. Dutta, T. Kamon and M. Tanaka, *Phys. Lett. B* **538** (2002) 121 [arXiv:hep-ph/0203069]; S. Baek, P. Ko and W. Y. Song, *Phys. Rev. Lett.* **89** (2002) 271801 [arXiv:hep-ph/0205259]; C. S. Huang and X. H. Wu, *Nucl. Phys. B* **657** (2003) 304 [arXiv:hep-ph/0212220]. S. Baek, Y. G. Kim and P. Ko, *JHEP* **0502** (2005) 067 [arXiv:hep-ph/0406033]; H. Baer, C. Balazs, A. Belyaev, J. K. Mizukoshi, X. Tata and Y. Wang, *JHEP* **0207** (2002) 050 [arXiv:hep-ph/0205325]; E. Lunghi, W. Porod and O. Vives, arXiv:hep-ph/0605177.
  20. J. R. Ellis, K. A. Olive and V. C. Spanos, *Phys. Lett. B* **624** (2005) 47 [arXiv:hep-ph/0504196].
  21. J. R. Ellis, K. A. Olive, Y. Santoso and V. C. Spanos, *JHEP* **0605**, 063 (2006) [arXiv:hep-ph/0603136].
  22. F. Abe *et al.* [CDF Collaboration], *Phys. Rev. D* **57** (1998) 3811; D. Acosta *et al.* [CDF Collaboration], *Phys. Rev. Lett.* **93** (2004) 032001 [arXiv:hep-ex/0403032]; V. M. Abazov *et al.* [D0 Collaboration], *Phys. Rev. Lett.* **94**, 071802 (2005) [arXiv:hep-ex/0410039]; The D0 Collaboration, D0note, 4733-CONF; <http://www-d0.fnal.gov/Run2Physics/WWW/results/prelim/B/B21/B21.pdf>; M. Herndon, The CDF and D0 Collaborations, FERMILAB-CONF-04-391-E. Published Proceedings 32nd International Conference on High-Energy Physics (ICHEP 04), Beijing, China, August 16-22, 2004; The CDF Collaboration, CDF note 7670; <http://www-cdf.fnal.gov/physics/new/bottom/050407.blessed-bsmumu/>.
  23. The CDF Collaboration, CDF Public Note 8176; <http://www-cdf.fnal.gov/physics/new/bottom/060316.blessed-bsmumu3/>
  24. J. L. Feng, K. T. Matchev and T. Moroi, *Phys. Rev. D* **61** (2000) 075005 [arXiv:hep-ph/9909334].
  25. M. Davier, S. Eidelman, A. Höcker and Z. Zhang, *Eur. Phys. J. C* **31** (2003) 503, hep-ph/0308213; see also K. Hagiwara, A. Martin, D. Nomura and T. Teubner, *Phys. Rev. D* **69** (2004) 093003, hep-ph/0312250; S. Ghozzi and F. Jegerlehner, *Phys. Lett. B* **583** (2004) 222, hep-ph/0310181; M. Knecht, hep-ph/0307239; K. Melnikov and A. Vainshtein, *Phys. Rev. D* **70** (2004) 113006 [arXiv:hep-ph/0312226]. J. de Troconiz and F. Yndurain, hep-ph/0402285; M. Passera, *Nucl. Phys. Proc. Suppl.* **155**, 365 (2006) [arXiv:hep-ph/0509372].
  26. J. R. Ellis, K. A. Olive, Y. Santoso and V. C. Spanos, *Phys. Rev. D* **71**, 095007 (2005) [arXiv:hep-ph/0502001].
  27. M. A. Shifman, A. I. Vainshtein and V. I. Zakharov, *Phys. Lett.* **78B**, 443 (1978); A. I. Vainshtein, V. I. Zakharov and M. A. Shifman, *Usp. Fiz. Nauk* **130**, 537 (1980).
  28. J. Ellis, K. Olive, Y. Santoso and V. Spanos, *Phys. Lett. B* **588** (2004) 7, hep-ph/0312262; J. Ellis, K. Olive and E. Vangioni, *Phys. Lett. B* **619** (2005) 30, astro-ph/0503023; J. Feng, S. Su and F. Takayama, *Phys. Rev. D* **70** (2004) 075019, hep-ph/0404231; *Phys. Rev. D* **70** (2004) 063514, hep-ph/0404198; J. Feng, A. Rajaraman and F. Takayama, *Phys. Rev. Lett.* **91** (2003) 011302, hep-ph/0302215.
  29. K. Hamaguchi, Y. Kuno, T. Nakaya and M. Nojiri, *Phys. Rev. D* **70** (2004) 115007, hep-ph/0409248; J. Feng and B. Smith, *Phys. Rev. D* **71** (2005) 015004 [Erratum-ibid. **D 71** (2005) 0109904], hep-ph/0409278; A. De Roeck, J. Ellis, F. Gianotti, F. Moortgat, K. Olive and L. Pape, hep-ph/0508198.
  30. V. Abazov *et al.* [D0 Collaboration], *Nature* **429** (2004) 638, hep-ex/0406031; P. Azzi *et al.* [CDF Collaboration, D0 Collaboration], hep-ex/0404010.
  31. CDF Collaboration, D0 Collaboration and Tevatron Electroweak Working Group, hep-ex/0507091.
  32. Tevatron Electroweak Working Group, hep-ex/0603039.
  33. T. E. W. Group, arXiv:hep-ex/0608032.
  34. J. Ellis, S. Heinemeyer, K. A. Olive and G. Weiglein, arXiv:hep-ph/0604180.
  35. LEP Higgs working group, *Phys. Lett. B* **565** (2003) 61, hep-ex/0306033; ALEPH, DELPHI, L3, OPAL Collaborations and LEP Working Group for Higgs boson searches, hep-ex/0602042.
  36. B. Allanach *et al.*, *Eur. Phys. J. C* **25** (2002) 113, hep-ph/0202233;
  37. G. Weiglein *et al.* [LHC / ILC Study Group], *Phys. Rept.* **426** (2006) 47, hep-ph/0410364.
  38. D. S. Akerib *et al.* [CDMS Collaboration], "Limits on spin-independent WIMP nucleon interactions from the two-tower *Phys. Rev. Lett.* **96**, 011302 (2006) [arXiv:astro-ph/0509259].